CFSRC COLLOQUIUM

Proceedings of the Cold-Formed Steel Research Consortium Colloquium
17-19 October 2022 (cfsrc.org)

Experimental Performance of Cold Form Flexural Members Under Distortional Buckling

Joshua A. Schultz[1], Christopher H. Raebel[2], Josh R. Buckholt[3], Daniel H. Raebel[4], William S. Newhoff[5]

Abstract

Recent developments for applications of cold formed steel elements that are increasingly slender have precipitated this investigation. The research focuses on the distortional buckling of C-shaped members in flexure, where the flange stiffeners are in compression and the web in tension. Previous research has been documented for this loading scenario for select shapes. However, there remains a lack of definitive experimental data into the behavior of these elements, particularly typical C-shape cross-sections. The initial results of this research suggest that the current distortional buckling strength curve found in the AISI code may not adequately address these cases. This research seeks to work in concert with these efforts to provide theoretical and experimental results that can be used by the task group to develop recommendations for designers. Three cross-sections at a 14, 16,18, 20 gauge for nominal spans of 3.05 m (10 ft) were tested, resulting in an experimental regime of 51 specimens. Experimental results are presented in terms of ultimate loads, P_{ts}, as well as elastic critical distortional buckling moment, M_{crd}, and yield moment, M_y.

1. General

Cold formed steel is used in an ever-widening range of applications due to favorable strength-to-weight and stiffness-to-weight ratios. As a result of these ratios, yielding is seldom the governing design consideration. Instead, nominal strength as the result of instability (local, distortional, and lateral-torsional buckling for members in strong-axis bending) is often the preeminent design concern.

The particular concern of this research is distortional buckling of C-shape members exposed to flexure about the weak axis. This can be encountered in a number of design applications, particularly for steel truss applications or other laterally unbraced configurations.

Consequently, this research evaluates flexural behavior of C-shapes about the weak axis, resulting in compression flanges and tension webs. Currently, AISI S100 Chapter F4 addresses I-, Z-, C-, and other open cross-section members that employ compression flanges with edge stiffeners [1]. However, AISI S100 Chapter F4 is based on strong axis experimental results [2]. Researchers have investigated the behavior of complex hat shapes and found distortional buckling to be a governing design consideration [3, 4]. To investigate the applicability of strong axis derived moment curves to weak axis applications, 51 specimens were tested to failure in distortional buckling about their weak axis. This research provides additional data for comparison to AISI S100-16 Figure C-F4.1-2 Performance of Distortional Buckling Prediction with Test Data on Common C- and Z-Sections in Bending as shown in Figure 1.

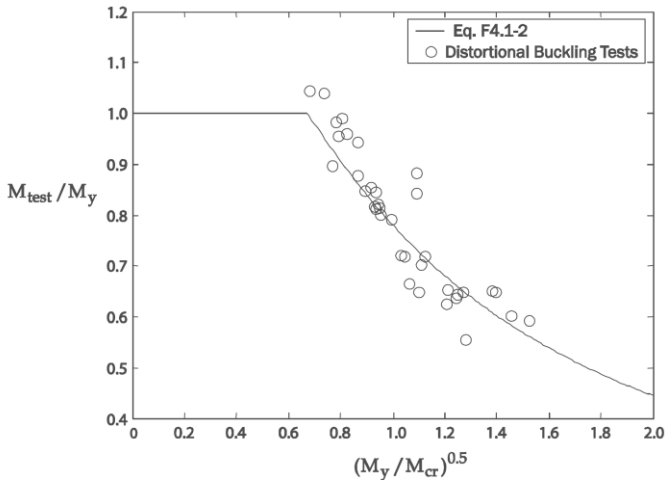

Figure 1: Performance of Distortional Buckling Prediction with Test Data on Common C- and Z-Sections in Bending per AISI S100-16 [1]

However, to-date there remains a dearth of experimental data regarding moment capacity of members that

[1] Associate Professor, Department of Civil Engineering, Gonzaga University, schultzj@gonzaga.edu
[2] Professor and Chair, Civil and Architectural Engineering and Construction Management, Milwaukee School of Engineering, raebel@msoe.edu
[3] Vice President/Principal, CSD Structural Engineers, jbuckholt@csd-eng.com
[4] Active Safety Feature Validation Engineer, General Motors, daniel.raebel@gm.com
[5] Research Assistant, Department of Civil Engineering, Gonzaga University, wnewhoff@zagmail.gonzaga.edu

experience distortional buckling when undergoing weak axis bending. As a result, the applicability of the current AISI S100 design curve is unknown. To address this, the experimental results are presented in terms of failure load, P_{ts}, as well as elastic critical distortional buckling moment, M_{crd}, and yield moment, M_y.

2. Experimental Program

The experimental program included 51 full-scale tests consisting of 3 tests for each of 17 different shapes conducted about the beam's weak axis. The tests were conducted using four-point bending setup as shown in Figure 2. The hydraulic actuators were instrumented with force and displacement transducers that measure in-line with the piston of the actuator. The loading frame, constructed of hot-rolled steel tube and being significantly stiffer than the cold form sections, applied lines of load orthogonal to the specimen at discrete points shown in Figures 2 and 3. The displacement was measured throughout the loading up to distortional buckling failure.

The test setup followed the AISI S911-17 standard [5] and each "b" value was different according to the specimen as shown in Figure 3. All S137 shapes had b=455 mm (18 in), S162 shapes had b=610 mm (24 in) and S200 and S300 had b=710 mm (28 in). The span, L, between support points, R, was held consistent at 2.8956 m (9.5 ft). Loads were applied by a single hydraulic load cell providing P_{ts} with a rigid spreader bar to distribute $P_{ts}/2$ to each point per Figure 3. The beams were unbraced and selected such that distortional buckling was the anticipated failure mode.

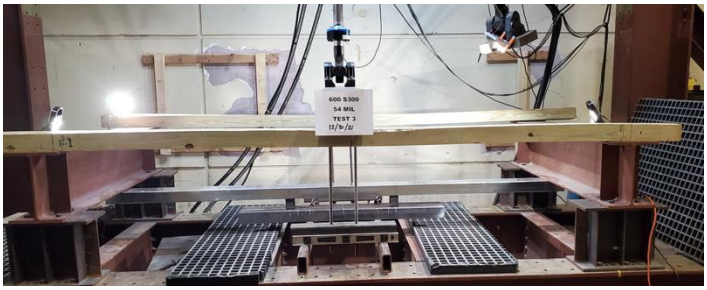

Figure 2: Typical Pre-test Configuration

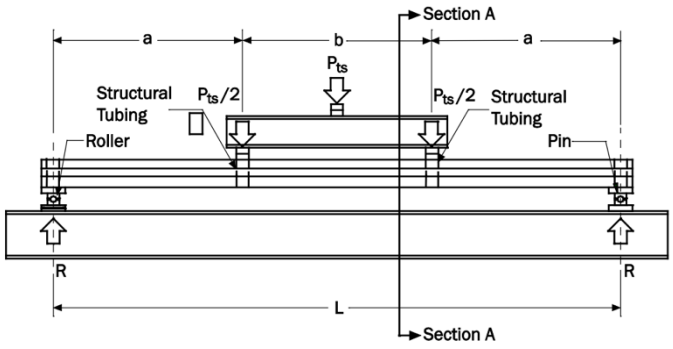

Figure 3: Experimental Set-up per AISI S911-17 [5]

Part of the experimental program included material testing of the specimens to determine actual material properties. The resulting material properties were obtained using tensile coupon testing by an independent and certified laboratory as reported in Table 1.

Table 1: Material Properties for Specimens

Specimen	Yield Strength (MPa)	Tensile Strength (MPa)
362_S137_33	400	476
362_S137_43	365	496
362_S137_54	434	524
362_S137_68	269	338
400_S162_33	400	469
400_S162_43	255	331
400_S162_54	462	538
400_S162_68	269	372
550_S200_33	262	359
550_S200_43	338	379
550_S200_54	448	517
550_S200_68	379	462
600_S200_33	462	538
600_S200_43	372	455
600_S200_54	400	476
600_S200_68	331	372
600_S300_54	427	503

3. Experimental Results

Every specimen was tested to failure and all members were designed to fail in distortional buckling. Each test provided force and displacement measurements read from the actuator's instrumentation. Figure 4 shows a typical specimen (600_S300_54) at completion of loading. All specimens were recorded during load applications and failure modes of distortional buckling were observed in-situ and independently verified later by reviewing the video.

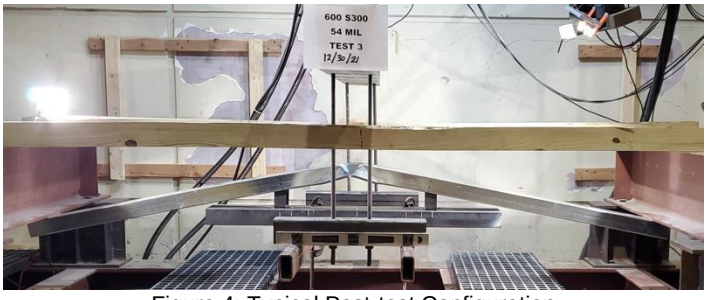

Figure 4: Typical Post-test Configuration

The load vs displacement plot for 550_S200 series specimens is shown below in Figure 5. Each of these plots clearly illustrates the key ranges labeled and discussed.

Initially, a force engagement range was observed while the actuator lifted the load frame and specimen until the

specimen engaged its end supports. This effectively brought the force to zero. The applied force magnitude measured within the engagement range consists of the weight of the specimen, load frame, threaded rod, spreader beam and the actuator's bottom clevis.

Next, a load accrual range occurred, where the specimen was slowly and continuously loaded. The specimen remained elastic during the load accrual range as evident by the linear region in the plots. This continued until the specimen reached its peak and the maximum experimental moment, M_{test}, was achieved. Distortional buckling was observed as the specimen approached its maximum moment. The initiation of buckling was evident on the load-displacement plots as the beginning of the nonlinear range prior to the maximum force. As buckling continued, the specimen's load capacity tapered off.

The corresponding ultimate load, P_{ts}, is provided for each specimen in Table 2. This value is used in conjunction with the distance from the load application point to the reaction point to determine the experimental distortional buckling moment capacity, M_{test}.

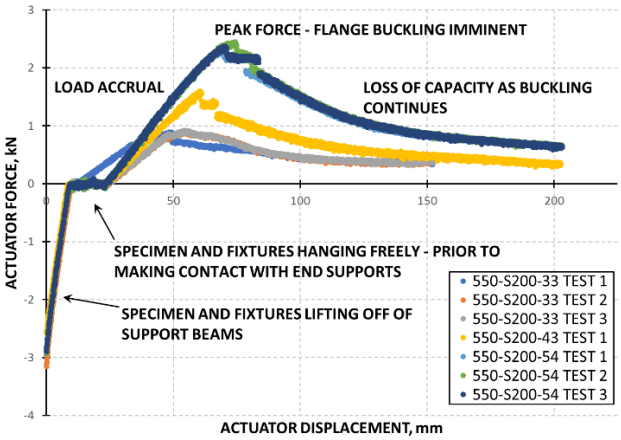

Figure 5: Load vs Displacement for 550_S200 Tests

Table 2: Distortional Buckling Failure Load

Specimen	P_{ts} (N)	Specimen	P_{ts} (N)
550_s200_33-1	466	362_s137_33-3	919
550_s200_33-2	446	362_s137_43-1	1573
550_s200_33-3	470	362_s137_43-2	1660
550_s200_43-1	809	362_s137_43-3	1461
550_s200_54-1	791	362_s137_54-1	2319
550_s200_54-2	754	362_s137_54-2	2425
550_s200_54-3	1389	362_s137_54-3	2360
550_s200_43-2	1319	362_s137_68-1	3479
550_s200_43-3	1378	362_s137_68-2	3413
550_s200_68-1	1789	362_s137_68-3	3439
550_s200_68-2	1781	400_s162_33-1	835
550_s200_68-3	1784	400_s162_33-2	951
600_s200_33-1	748	400_s162_33-3	831
600_s200_33-2	823	400_s162_43-1	1335
600_s200_33-3	799	400_s162_43-2	1343
600_s200_43-1	1003	400_s162_43-3	1381
600_s200_43-2	1022	400_s162_54-1	2089
600_s200_43-3	1000	400_s162_54-2	2096
600_s200_54-1	1509	400_s162_54-3	2165
600_s200_54-2	1520	400_s162_68-1	3789
600_s200_54-3	1495	400_s162_68-2	3747
600_s200_68-1	2055	400_s162_68-3	3738
600_s200_68-2	2011	600_s300_54-1	2945
600_s200_68-3	1955	600_s300_54-2	3018
362_s137_33-1	866	600_s300_54-3	3078
362_s137_33-2	914		

4. Numerical Analyses

CUFSM v4.03 [6] was used to generate theoretical elastic critical buckling M_{crd} values as shown in Table 3. CUFSM uses the finite strip method to determine buckling response curves based on material and geometry. The experimental distortional buckling moment, M_{test}, was then normalized to its yield moment, M_y, calculated using the measured yield strength, F_y, of the respective cross section. This normalized experimental distortional buckling moment capacity (M_{test}/M_y) was then plotted as a function of its distortional buckling slenderness, $\sqrt{M_y/M_{crd}}$.

Table 3: Elastic Distortional Buckling Moment, M_{crd}

Specimen	M_{CRD} (kN-m)
362_s137_33	0.515867
362_s137_43	0.901778
362_s137_54	1.457167
362_s137_68	2.393813
400_s162_33	0.684463
400_s162_43	1.184874
400_s162_54	1.904249
400_s162_68	3.099065
550_s200_33	0.85594
550_s200_43	1.479313
550_s200_54	2.371103
550_s200_68	3.841603
600_s200_33	0.867149
600_s200_43	1.498633
600_s200_54	2.403191
600_s200_68	3.905778
600_s300_54	2.127507

The resulting values are presented in Figure 6 which shows the current experimental results compared to the AISI S100 Eq. F4.1-2. Note that the AISI Eq. F4.1-2 tends to overestimate the capacity due to elastic distortional buckling moment. For larger ratios of $\sqrt{M_y/M_{crd}}$ the overestimation can be significant.

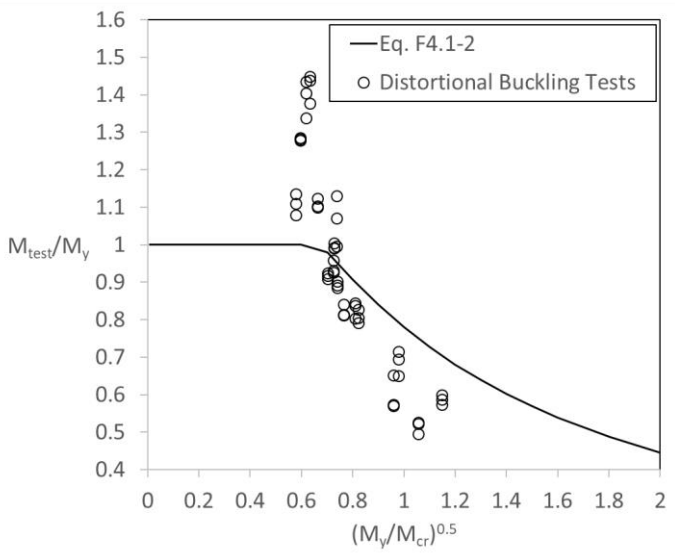

Figure 6: Experimental Results For Distortional Buckling Shown with Eq. F4.1-2

7. Conclusions

Experimental tests were conducted on 51 C-shaped specimens that were pre-selected to fail in distortional buckling. The resulting load-displacement plots were determined for all specimens and the ultimate load at buckling failure was obtained. The resulting experimental distortional buckling capacities were compared to the AISI S100 Chapter F4 buckling curve.

From these results it is observed that the AISI S100 F4 equations tend to overestimate the capacity for C-shapes when bent about the weak axis. Further work on reliability analysis and development of appropriate modifications to the current code equations is recommended.

8. Acknowledgments

This research initiative was supported by the Small Project Fellowship Program through the American Iron and Steel Institute. SCAFCO also provided material support by donating the specimens used for experimental testing. The authors thank these organizations for their support.

The authors would also like to thank Mr. Bob Glauz for fruitful discussions and valuable input throughout the project.

References

[1] AISI S100-16, North American Specification for the Design of Cold-Formed Steel Structural Members. Washington, DC, U.S.A.: AISI, 2016.

[2] Yu, Cheng, and Benjamin W. Schafer. "Local buckling tests on cold-formed steel beams." (2002).

[3] Nuttayasakul, N., and W. S. Easterling. "Cold-formed steel flexural members undergoing distortional and Euler buckling." Proc., Structural Stability Research Council (2003): 339-355.

[4] Baur, S. W., and R. A. LaBoube. "Behavior of complex hat shape cold-formed steel members." Proc., Structural Stability Research Council, Structural Stability Research Council (2001): 403-417.

[5] AISI S911-17, North American Specification for the Design of Cold-Formed Steel Structural Members. Washington, DC, U.S.A.: AISI, 2016

[6] Li, Zhanjie, and Benjamin W. Schafer. "Buckling analysis of cold-formed steel members with general boundary conditions using CUFSM conventional and constrained finite strip methods." (2010).